Dependence of the interfacial Dzyaloshinskii-Moriya interaction, perpendicular magnetic anisotropy, and damping in Co-based systems on the thickness of Pt and Ir layers

D. Ourdani,[1] Y. Roussigné,[1] S. M. Chérif,[1] M. S. Gabor,[2,*] and M. Belmeguenai[1,†]

[1]*Université Sorbonne Paris Nord, Laboratoire des Sciences des Procédés et des Matériaux (LSPM), Centre national de la recherche scientifique (CNRS), UPR 3407, F-93430 Villetaneuse, France*

[2]*Center for Superconductivity, Spintronics and Surface Science, Physics and Chemistry Department, Technical University of Cluj-Napoca, Str. Memorandumului No. 28, RO-400114 Cluj-Napoca, Romania*

(Received 25 June 2021; revised 9 August 2021; accepted 1 September 2021; published 21 September 2021)

Ir and Pt thickness dependences of the interfacial Dzyaloshinskii-Moriya interaction (iDMI), the perpendicular magnetic anisotropy (PMA), and the damping in Co-based systems grown by sputtering on Si substrates, using Ir or Pt under or overlayer of variable thickness ($0 \leqslant t_{Pt} \leqslant 3.5$ nm and $0 \leqslant t_{Ir} \leqslant 1.5$ nm), were investigated using Brillouin light scattering. Vibrating sample magnetometry measurements revealed a significant decrease of the areal magnetic moment at saturation as the thickness t_{Pt} or t_{Ir} of the overlayer increases, most likely due to the increasing intermixing. The intermixing, found to be negligible for Ir and Pt underlayers, is stronger for Ir than Pt overlayers. Damping measurements for Pt-based systems allowed us to conclude with the strong spin-pumping contribution. The analysis of the t_{Pt} dependence of damping, within the spin-pumping model, allowed us to determine the spin-diffusion length of Pt, found to be greater when Pt is used as an underlayer. The t_{Pt} dependence of the effective PMA and iDMI constants, for which similar trends to that of damping were observed, were qualitatively analyzed to separate the contribution of each interface with Co. It was found that these constants are stronger when Co is grown on Pt, most probably due to weaker intermixing at the Pt/Co interface. Linear dependence of damping vs the PMA effective constant was evidenced, confirming their relationship with spin-orbit coupling (SOC). A linear variation of the PMA effective constant vs the iDMI constant was observed in systems using Pt underlayer, whereas quadratic or linear correlations are possible when Pt is used as an overlayer, probably due to change of the interface SOC by the strong intermixing at the Co/Pt interface. The qualitative analysis of the Ir thickness dependence of iDMI and PMA constants revealed a significant (weak) contribution of the Ir/Co interface to PMA (iDMI). The surface iDMI constant of the Co/Ir interface was estimated to be 0.4 ± 0.1 pJ/m, which confirms the similar iDMI sign of Co/Ir and Co/Pt interfaces.

DOI: 10.1103/PhysRevB.104.104421

I. INTRODUCTION

Spin-orbit coupling (SOC), interaction which links the orbital motion of electrons to their spin, triggers several important phenomena in magnetism such as magnetic anisotropy, damping, or magnetostriction. The ultrathin character of the magnetic layer conjugated to the strong spin-orbit interaction greatly enhances these phenomena and induces other fascinating interface effects in heterostructures incorporating heavy metals (HMs) in contact with a ferromagnetic (FM) layer [1]. For instance, the interface contribution to perpendicular magnetic anisotropy (PMA), which is one of the most important properties of magnetic materials due to its potential applications [2–4], gets markedly stronger as the FM thickness is decreased, and consequently, the magnetic easy axis changes from the film plane to the film normal. Moreover, recent advances in magnetism demonstrated experimentally the existence of an antisymmetric interfacial exchange interaction in such FM/HM-based systems known as the interfacial Dzyaloshinskii-Moriya interaction (iDMI) [5,6]. The iDMI manifests itself as an internal magnetic field favoring a chiral arrangement of the magnetization, such as a homochiral Néel domain wall in PMA systems [7] and skyrmions [8]. Sizeable iDMI and PMA are essential components in generating magnetic skyrmions, which can be used in high-density digital technologies for racetrack memory [9] and logic devices [10]. Moreover, for such devices, where smaller, faster, and efficient are the main features, the damping constant is of utmost importance since it governs the magnetization dynamics such as the speed of magnetization reversal [11] and domain-wall motion [12].

The strength of iDMI, PMA, and damping is linked to the magnitude of the SOC and the degree of symmetry breaking for iDMI. Engineering aiming to enlarge the strength of these parameters could be achieved by optimizing the interface quality, changing the materials adjacent to the FM layer, and inserting ultrathin layers at the interfaces. Physical origins of the SOC-related phenomena were studied by variation of the FM thin film thickness. However, such investigation needs to change the HM and thus hardly allows evidencing correlation between these SOC-related phenomena since very few heavy materials were found to induce iDMI. Furthermore, varying

*mihai.gabor@phys.utcluj.ro
†belmeguenai.mohamed@univ-paris13.fr

under or overlayer materials could completely change interfaces, and thus origins and mechanisms responsible for these three interface and SOC-related effects [13]. Additionally, the dependence of the magnetic properties on thickness of the different under and overlayer heavy materials, especially for iDMI and PMA, was not systematically studied. Such investigations are powerful means to evidence any correlation between these parameters and to define their range and the atomic interface planes involved in these effects. Moreover, it could help in the control of damping, PMA, and iDMI and would significantly advance spintronics from both fundamental research and applied perspectives. In this paper, we combined Brillouin light scattering (BLS) and vibrating sample magnetometry (VSM) to experimentally investigate the heavy material thickness dependence of PMA, iDMI, and damping constants in HM/Co-based systems, where HM under or overlayers are Ir or Pt.

II. SAMPLES AND EXPERIMENTAL TECHNIQUES

All samples studied here, consisting mainly of Pt, Ir, and Co stacks, were grown at room temperature using a magnetron sputtering system, having a base pressure $<2 \times 10^{-8}$ Torr, on thermally oxidized Si/SiO_2 substrates. Two sets of samples were grown. In the first set, Pt was used as under or overlayer, and its thickness was varied in the range of 0–3.5 nm ($0 \leqslant t_{Pt} \leqslant 3.5$ nm). The considered stacks for this type of sample were

(i) $Si/SiO_2/Ta(2.5)/Cu(3)/Pt(t_{Pt})/Co(1.4)/Cu(3)/Ta(2.5)$,

(ii) $Si/SiO_2/Ta(2.5)/Cu(3)/Co(1.4)/Pt(t_{Pt})/Cu(3)/Ta(2.5)$,

where numbers in parentheses represent the thickness in nanometers.

In the second set, the thickness of the Ir under or overlayer was varied in the range of 0–1.5 nm ($0 \leqslant t_{Pt} \leqslant 1.5$ nm). Four types of samples were considered for this second set, having the following stacks:

(i) $Si/SiO_2/Ta(2.5)/Pt(3)/Ir(t_{Ir})/Co(1.4)/Cu(3)/Ta(2.5)$,

(ii) $Si/SiO_2/Ta(2.5)/Pt(3)/Co(1.4)/Ir(t_{Ir})/Cu(3)/Ta(2.5)$,

(iii) $Si/SiO_2/Ta(2.5)/Pt(3)/Cu(3)/Ir(t_{Ir})/Co(1.4)/Cu(3)/Ta(2.5)$,

(iv) $Si/SiO_2/Ta(2.5)/Pt(3)/Cu(3)/Co(1.4)/Ir(t_{Ir})/Cu(3)/Ta(2.5)$.

All metallic films were direct current sputtered in an Ar pressure of 1.5 mTorr. Pt and Ir are HMs having high SOC and showing large iDMI.

For each sample, the hysteresis loops under in-plane and perpendicular applied magnetic fields were measured using VSM, and the nominal magnetization at saturation (M_{sn}) was then determined considering the nominal thickness of Co. BLS [14], under in-plane applied magnetic field, was used in Damon-Eshbach configuration to investigate iDMI, PMA, and damping. For this, the recorded spectra were fitted with a Lorentzian to obtain the Stokes (S) and anti-Stokes (aS) line frequencies and their full width at half maximum height (δF_S and δF_{aS}). Two kinds of experiments were carried out here: (i) for PMA and damping investigation, spectra at fixed wave vector ($k_{sw} = 8.08\,\mu m^{-1}$ and therefore, incident angle of 20°) and variable in-plane applied magnetic field (in the range 1–13 kOe) were measured, then the field dependence of the mean frequency [$F = (F_S + F_{aS})/2$] and the mean linewidth δF[$\delta F = (\delta F_S + \delta F_{aS})/2$] were used to deduce the effective magnetization and damping constant, respectively. For the second kind of experiments, spectra were recorded at fixed in-plane applied magnetic field (sufficiently strong to saturate the magnetization in the film plane) and variable spin wave vector (in the range $k_{sw} = 8.08$–$20.45\,\mu m^{-1}$, incident angle in the range 20°–60°). The variation of the frequency mismatch between S and aS lines ($\Delta F = F_S - F_{aS}$) vs the spin wave (k_{sw}) allowed us to characterize the iDMI strength, as it will be shown below. For the iDMI constant, k_{sw} was varied over the available range for better precision. However, for damping and PMA determination, k_{sw} was fixed at a weaker value ($8.08\,\mu m^{-1}$) to minimize the iDMI contribution to the linewidth and decrease the accumulation time during spectra recording since the signal-to-noise ratio decreases with increasing field and k_{sw}.

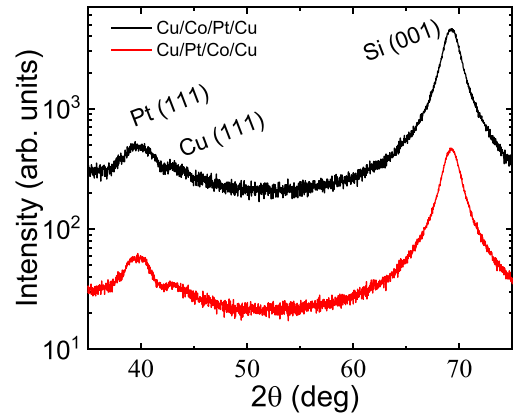

FIG. 1. $2\theta/\omega$ x-ray diffraction patterns recorded for Cu(3)/Pt(3.5)/Co(1.4)/Cu(3) and Cu(3)/Co(1.4)/Pt(3.5)/Cu(3) samples. Numbers in parentheses give the nominal thicknesses in nanometers.

III. RESULTS AND DISCUSSIONS

A. Structural properties

To study the crystal structure of the samples, we performed x-ray diffraction experiments. Figure 1 shows the $2\theta/\omega$ diffraction patterns recorded for two representative samples from series 1, with a thickness of the Pt layer of 3.5 nm. The patterns show a main peak corresponding to the Si substrate (001) reflection and another main peak at ∼39.7°, corresponding to the Pt (111) reflection. The small shoulder at ∼43.3° could be attributed to the Cu (111) reflection. Due to its relatively low thickness and atomic scattering factor, no peaks belonging to the Co layer were observed. Furthermore, no peaks issued from the Ta layers were detected, indicating that the films are in an amorphous or nanocrystalline state. The lack of other peaks except the (111) reflections indicates that Pt, Cu, and most likely, Co layers have a (111) out-of-plane texture, as expected for face-centered cubic metals [15].

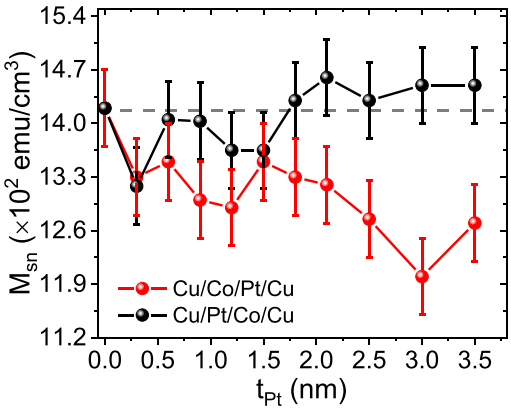

FIG. 2. Variations of the nominal magnetization at saturation (M_{sn}), calculated by dividing the measured vibrating sample magnetometry (VSM) magnetic moment at saturation to the nominal volume (surface × nominal thickness of Co) of the Co film for Cu/Co(1.4 nm)/Pt(t_{Pt}) and Cu/Pt(t_{Pt})/Co(1.4 nm)/Cu, vs the Pt thickness (t_{Pt}). Dashed gray line refers to the magnetization at saturation (M_s) of bulk Co.

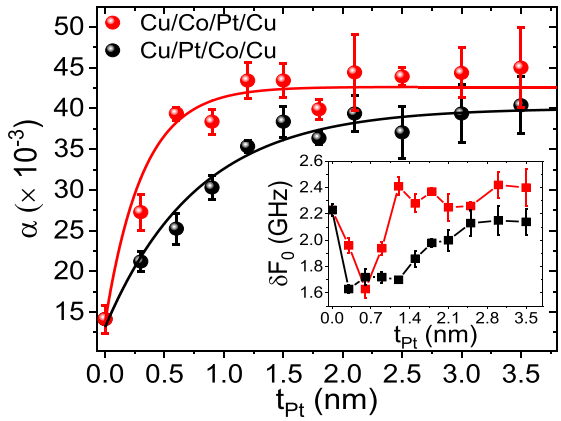

FIG. 3. Variations of the Gilbert effective damping (α) vs the Pt thickness for Cu/Co(1.4 nm)/Pt(t_{Pt}) and Cu/Pt(t_{Pt})/Co(1.4 nm)/Cu systems. Symbols are experimental data, and solid lines are fits using Eq. (2). The inset shows the variation of the corresponding inhomogeneous residual linewidth δF_0 vs the Pt thickness.

Interestingly, for both structures, the Pt layer (111) diffraction maximum is at roughly the same 2θ angle of ∼39.7°, corresponding to the value for bulk Pt. Having in view the relatively large lattice misfit of Pt grown on Co (9.6%) and of Pt grown on Cu (7.8%), this indicates that strains are relaxed through the formation of misfit dislocations. The Pt peaks were fitted using pseudo-Voigt functions, and mean grain size was determined using the well-known Scherrer equation [16,17], which gives a value of ∼3.6 nm for the Cu/Pt/Co/Cu and ∼3 nm for the Cu/Co/Pt/Cu. This value is essentially the same as the Pt layer thickness for the Cu/Pt/Co/Cu sample and is lower than the Pt layer thickness for the Cu/Co/Pt/Cu sample, most likely due to intermixing at the Co/Pt interface, as we will argue below.

B. Effect of Pt capping or buffer layer thickness

This section is devoted to the investigation of the Pt thickness (t_{Pt}) effect on damping, PMA, and iDMI in Si/SiO$_2$/Ta(2.5)/Cu(3)/Pt(t_{Pt})/Co(1.4)/Cu(3)/Ta(2.5), referred to as Cu/Pt(t_{Pt})/Co(1.4 m)/Cu, and Si/SiO$_2$/Ta(2.5)/Cu(3)/Co(1.4)/Pt(t_{Pt})/Cu(3)/Ta(2.5), denoted as Cu/Co(1.4 nm)/Pt(t_{Pt})/Cu, where numbers in parentheses for both systems give the nominal thicknesses in nanometers.

Figure 2 shows the VSM nominal magnetizations at saturation (M_{sn}) for Cu/Pt(t_{Pt})/Co(1.4 nm)/Cu and Cu/Co(1.4 nm)/Pt(t_{Pt})/Cu. Here, M_{sn} values were calculated by dividing the magnetic moment at saturation m_s, directly measured by VSM, by the nominal volume of the Co film. The two systems markedly behave differently: while a slight variation of M_{sn} is observed for Cu/Pt(t_{Pt})/Co(1.4 nm)/Cu, M_{sn} decreases significantly with increasing t_{Pt} for Cu/Co(1.4 nm)/Pt(t_{Pt})/Cu due to the increasing intermixing at the Co/Pt interface. This suggests that the top and bottom Pt layers contribute differently to intermixing and thus to the resulting magnetic dead layer at the interface: the Pt underlayer does not induce magnetic dead layer, whereas it induces significant magnetic dead layer when it is grown on top of Co. Indeed, in contrast to light atoms of Cu, heavy atoms such as Pt are more energetic and are expected to diffuse more in Co, leading to higher interface mixing. Therefore, due to immiscibility of the Cu and Co [18], the nominal magnetization at saturation corresponding to zero Pt (1420 emu/cm^3), which is in good agreement with the magnetization at saturation (M_s) of bulk Co (1430 emu/cm^3), will be used as M_s in this paper, especially when deducing some parameters characterizing the SOC-related effects. Note the slightly higher M_{sn} values for $t_{Pt} > 1.5$ nm with respect to 1420 emu/cm^3 for Cu/Pt(t_{Pt})/Co(1.4 nm)/Cu most probably due to the proximity induced magnetization (PIM) at the Pt/Co interface.

BLS can be used to investigate the Gilbert damping constant α by measuring the field dependence of the full width at half maximum height of S and aS lines (δF_S and δF_{aS}). It is worth mentioning that the BLS linewidth contains an additional instrumental contribution resulting from the tandem Fabry-Perot interferometer (∼1% of the measured frequency, i.e., ≈0.1 GHz) and the lens aperture (∼0.1 GHz). These instrumental contributions are magnetic field independent. The observed linewidth variations which are related to the Gilbert damping constant introduce a contribution proportional to the applied field. Therefore, to deduce the Gilbert damping constant α, the field dependence of the mean linewidth δF, defined as $\delta F = (\delta F_S + \delta F_{aS})/2$, is fitted using Eq. (1):

$$\delta F = \delta F_0 + \frac{\gamma}{2\pi} 2\alpha H, \tag{1}$$

where δF_0 is the inhomogeneous residual linewidth, and γ is the gyromagnetic ratio.

Figure 3 shows the Pt thickness dependence of α for Cu/Pt(t_{Pt})/Co(1.4 nm)/Cu and Cu/Co(1.4 nm)/Pt(t_{Pt})/Cu, where an exponential saturation is observed. Note the higher values of α and its faster saturation with Pt thickness for Cu/Co(1.4 nm)/Pt(t_{Pt})/Cu. These trends are most likely due to the spin-pumping contribution to damping at Pt/Co and

Co/Pt interfaces. In fact, in addition to the exponential dependence of α, as t_{Pt} increases, the magnetic dead layer thickness increases, reducing the effective thickness of Co, leading to higher damping due to spin pumping, especially for Cu/Co(1.4 nm)/Pt(t_{Pt})/Cu, where thicker magnetic dead layer is expected. Therefore, the t_{Pt} dependence of α was fitted by Eq. (2) [19], describing the damping of a FM layer as a function of the thickness of the adjacent nonmagnetic layer (Pt here):

$$\alpha = \alpha_{\mathrm{Co}} + \frac{g\mu_B}{4\pi M_s t_{\mathrm{eff}}} g_{\mathrm{eff}}^{\uparrow\downarrow}\left[1 - \exp\left(-\frac{2t_{\mathrm{Pt}}}{\lambda_{\mathrm{SD}}}\right)\right], \qquad (2)$$

where μ_B is the Bohr magneton, α_{Co} is the Gilbert damping constant of the bulk Co, g is the Landé factor of Co, λ_{SD} is Pt spin diffusion length, and $g_{\mathrm{eff}}^{\uparrow\downarrow}$ is the effective spin-mixing conductance. It is worth mentioning that the higher α values for Cu/Co(1.4 nm)/Pt(t_{Pt})/Cu could also be attributed to the higher intermixing occurring at the top Co/Pt interface.

By fitting the experimental t_{Pt} dependence of α_{Co} with Eq. (2), we obtained $g_{\mathrm{eff}}^{\uparrow\downarrow} = 32 \pm 2\,\mathrm{nm}^{-2}$ and $\alpha_{\mathrm{Co}} = (1.3 \pm 0.2) \times 10^{-2}$ for both systems, and we determine $\lambda_{\mathrm{Pt}} = 1.55 \pm 0.28$ nm and 0.8 ± 0.1 nm for Cu/Pt(t_{Pt})/Co(1.4 nm)/Cu and Cu/Co(1.4 nm)/Pt(t_{Pt})/Cu, respectively. This value of α_{Co} is slightly higher than that of the bulk Co ($\alpha_{\mathrm{Co}} = 0.01$) [20], whereas the $g_{\mathrm{eff}}^{\uparrow\downarrow}$ value is slightly lower than that reported by Zhu *et al.* ($45\,\mathrm{nm}^{-2}$) [21]. Furthermore, the obtained value of λ_{Pt} for the Cu/Pt(t_{Pt})/Co(1.4 nm)/Cu system is in good agreement with the reported one (1.2 nm) by Vlaminck *et al.* [22]. The reduced λ_{Pt} for Cu/Co(1.4 nm)/Pt(t_{Pt})/Cu could be attributed to strong scattering of the injected spin current in the intermixed layer formed at the interface.

In Fig. 3, solid lines, referring to fits using Eq. (2), were obtained using constant M_s ($1420\,\mathrm{emu/cm^3}$), $g = 2.23$ and $t_{\mathrm{eff}} = t_{\mathrm{Co}} = 1.4$ nm, ignoring thus the variation of M_{sn} vs t_{Pt} and therefore the existence of any magnetic dead layer, especially for Cu/Co(1.4 nm)/Pt(t_{Pt})/Cu. However, according to Eq. (2), the spin-pumping-introduced damping depends on $M_s \times t_{\mathrm{eff}}$, which is directly measured by VSM and corresponding to $M_{sn} \times t_{\mathrm{Co}}$ ($M_{sn} \times t_{\mathrm{Co}} = M_s \times t_{\mathrm{eff}}$). Therefore, the experimental data of Fig. 3 were compared with the calculated ones (not shown here) using Eq. (2), $M_{sn} \times t_{\mathrm{Co}}$ and the abovementioned values of $\alpha_{\mathrm{Co}} = 1.3 \times 10^{-2}$ and $g = 2.23$, whereas $g_{\mathrm{eff}}^{\uparrow\downarrow}$ and λ_{SD} are fitting parameters. This allowed us to reproduce well the pronounced fluctuations of α for high t_{Pt} (in the saturation regime) in the Cu/Co(1.4 nm)/Pt(t_{Pt})/Cu system, thus confirming their physical origin. Furthermore, the obtained parameters with this fit procedure revealed that λ_{SD} of Cu/Co(1.4 nm)/Pt(t_{Pt})/Cu system decreases from 0.8 ± 0.1 nm, when constant M_s is used, down to 0.6 ± 0.1 nm for the fit with variable M_s. In contrast, no significant variation in λ_{SD} of Cu/Pt(t_{Pt})/Co(1.4 nm)/Cu was observed, suggesting an increase of spin scattering at the Co/Pt interface, thus decreasing λ_{SD}.

To investigate the PMA, the field dependence of the mean frequency of each sample, defined as $F = (F_{\mathrm{S}} + F_{\mathrm{aS}})/2$, was fitted by Eq. (3), and the effective magnetization ($4\pi M_{\mathrm{eff}} = 4\pi M_s - \frac{2K_{\mathrm{eff}}}{M_s}$, where K_{eff} is the effective PMA constant) was deduced:

$$F = \frac{\gamma}{2\pi}\sqrt{\left[H + Jk_{sw}^2 + P(k_{sw}t_{\mathrm{eff}})4\pi M_s\right]\left[H + Jk_{sw}^2 - P(k_{sw}t_{\mathrm{eff}})4\pi M_s + 4\pi M_{\mathrm{eff}}\right]}, \qquad (3)$$

where H is the in-plane applied magnetic field, t_{eff} is the effective Co thickness (the Co nominal thickness reduced by the magnetic dead layer thickness), $J = \frac{2A_{ex}}{M_s}$, where A_{ex} is the exchange stiffness constant of Co, $\gamma/(2\pi) = 31.2\,\mathrm{GHz/T}$ is the gyromagnetic ratio, and $P(k_{sw}t_{\mathrm{eff}})$ is defined in Ref. [23].

Figure 4(a) shows the Pt thickness dependence of $4\pi M_{\mathrm{eff}}$ for Cu/Pt(t_{Pt})/Co(1.4 nm)/Cu and Cu/Co(1.4 nm)/Pt(t_{Pt})/Cu systems, where M_{eff} decreases with increasing t_{Pt}, suggesting the increase of the perpendicular effective anisotropy constant (K_{eff}). Note the lower saturation of M_{eff} at thicker Pt for Cu/Pt(t_{Pt})/Co(1.4 nm)/Cu and its positive values, indicating that K_{eff} is not sufficient to overcome the demagnetizing contribution favoring the in-plane easy axis. Therefore, for the investigated t_{Pt} range, the samples are not spontaneous perpendicularly magnetized.

Using a constant value for $M_s = 1420\,\mathrm{emu/cm^3}$ for the entire t_{Pt} range, K_{eff} was deduced from the experimental data of Fig. 4(a), as shown in Fig. 4(b). One should mention the higher K_{eff} at saturation (for the thickest Pt layers) for Cu/Pt(t_{Pt})/Co(1.4 nm)/Cu than Cu/Co(1.4 nm)/Pt(t_{Pt})/Cu, suggesting asymmetry between the two interfaces: the bottom interface, i.e., when the Co layer is deposited on a Pt buffer layer, induces significantly higher K_{eff}. Here, K_{eff} is usually described by the phenomenological relationship $K_{\mathrm{eff}} = K_v + \frac{K_s}{t_{\mathrm{eff}}}$, where K_s and K_v are the PMA surface and volume constants, respectively. It is considered that the PMA in Pt/Co multilayers may arise from the hybridization of Co and Pt orbitals or from magnetoelastic effects [18,24].

Our data show thus that the top Co/Pt interface has a much lower contribution to interfacial anisotropy than the bottom Pt/Co one. Indeed, intermixing occurring at the top Co/Pt interface can deteriorate the K_{eff} [18,25], as confirmed by Bandiera *et al.* [25], who reported that the effective magnetic anisotropy of sputtered Pt/Co/Pt can be doubled by inserting a Cu layer between Co and Pt at the Co/Pt top interface, limiting the intermixing occurring at this interface. Moreover, the slower and the faster saturation of K_{eff} for Cu/Pt(t_{Pt})/Co(1.4 nm)/Cu and Cu/Co(1.4 nm)/Pt(t_{Pt})/Cu, respectively, cannot be attributed the variation of M_{sn} and thus to the change of the magnetic dead layer, especially for Cu/Co(1.4 nm)/Pt(t_{Pt})/Cu since M_{sn} for these systems varies (decreases) continuously as t_{Pt} increases. Therefore, it is most likely that, as t_{Pt} increases, both K_v and K_s change, as reported by Guo *et al.* [26], and then saturates at a given t_{Pt} which depends on the interface quality. Indeed, changing the under or overlayer can modify the Co layer texture, crystal orientation, stress, roughness, or microstructure, thus affecting the anisotropy of the stack. Moreover, one must consider that Co

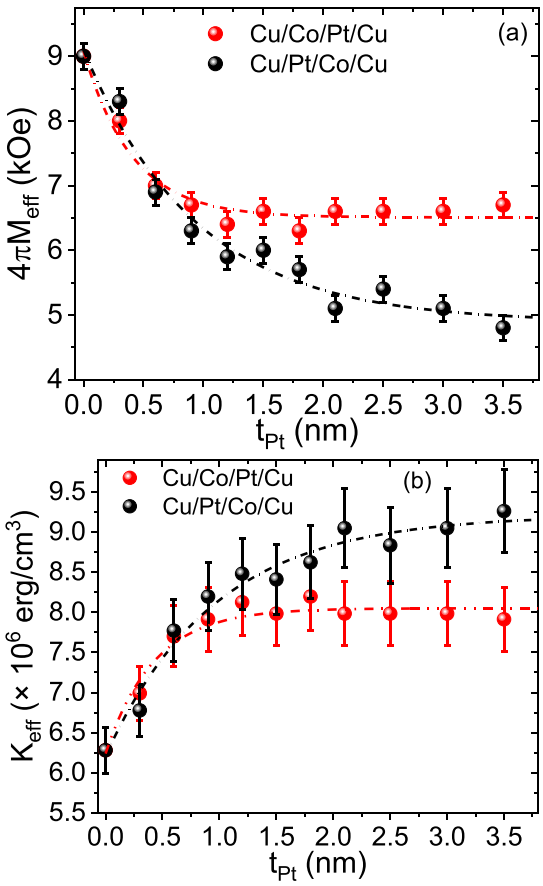

FIG. 4. Variations of (a) the effective magnetization ($4\pi M_{\text{eff}}$) and (b) the effective perpendicular anisotropy constant (K_{eff}) vs the Pt thickness for Cu/Co(1.4 nm)/Pt(t_{Pt}) and Cu/Pt(t_{Pt})/Co(1.4 nm)/Cu systems. $4\pi M_{\text{eff}}$ values were extracted from the fit of field dependence of the mean frequency for S and aS lines with Eq. (3). Symbols refer to experimental data, while solid lines are fits using Eq. (5) and parameters in Table I.

is subjected to different degrees of strain when grown on Pt or Cu. For example, the lattice misfit between Pt and Co is relatively large (∼9.6%). Such a degree of strain cannot be accommodated in the 1.4 nm Co layer and is relaxed through the formation of misfit dislocations [15]. The residual strain resulting from this plastic deformation can act as an apparent magnetoelastic-induced surface anisotropy [27]. In the case of the Co layer grown on Cu, the lattice misfit is much lower, ∼1.9%. For such a lattice misfit, the Co layer might grow pseudomorphic, or most likely, the strain might be relaxed through plastic deformation [28]. Having in view the lower lattice misfit as compared with Co grown on Pt, it is expected that the residual strain resulting from the plastic deformation will produce a much lower apparent magnetoelastic-induced surface anisotropy.

To qualitatively analyze the data and to estimate the interface contribution to M_{eff}, we assumed that $M_s = 1420\,\text{emu/cm}^3$, Pt under or overlayer induces a magnetic dead layer thickness without affecting M_s, and we consider that the volume contribution to PMA is equal to the bulk magnetocrystalline anisotropy of the hexagonal Co ($K_v = 5.1 \times 10^6\,\text{erg cm}^{-3}$) [29]. For each system, the PMA constant is written as $K_{\text{eff}} = K_v + \frac{K_s^{\text{top}}}{t_{\text{eff}}} + \frac{K_s^{\text{Bot}}}{t_{\text{eff}}}$, where K_s^{Bot} and K_s^{top} are surface PMA constants of the top and bottom interfaces with Co, respectively. Using the A_0 value (corresponding to $t_{\text{Pt}} = 0$ and thus to the Cu/Co/Cu system) for K_{eff} indicated in Table I, one can write $K_{\text{eff}} = A_0 = K_v + \frac{K_s^{\text{Cu/Co}}}{t_{\text{eff}}} + \frac{K_s^{\text{Co/Cu}}}{t_{\text{eff}}} = 6.23 \times 10^6\,\text{erg/cm}^3$. This leads to $K_s^{\text{Cu/Co}} = \frac{1}{2} \times t_{\text{eff}}(A_0 - K_v)$, where $t_{\text{eff}} = t_{\text{Co}} = 1.4\,\text{nm}$ since no magnetic dead layer is introduced by Co/Cu and Cu/Co interfaces. It is worth mentioning that the factor 2 in the above expression of $K_s^{\text{Cu/Co}}$ is introduced to assume symmetric Co/Cu and Cu/Co interfaces. This gives $K_s^{\text{Cu/Co}} = K_s^{\text{Co/Cu}} = 0.08 \pm 0.007\,\text{erg/cm}^2$. In a similar way, and considering K_{eff} values at saturation (given by $A_0 + A_1$ in Table I) for Cu/Pt(t_{Pt})/Co(1.4 nm)/Cu and Cu/Co(1.4 nm)/Pt(t_{Pt})/Cu systems, K_{eff} of the Cu/Pt(t_{Pt})/Co(1.4 nm)/Cu system can be written as $K_{\text{eff}} = A_0 + A_1 = K_v + \frac{K_s^{\text{Pt/Co}}}{t_{\text{eff}}} + \frac{K_s^{\text{Co/Cu}}}{t_{\text{eff}}}$. Therefore, we infer $K_s^{\text{Pt/Co}} = t_{\text{eff}}(A_0 + A_1 - K_v) - K_s^{\text{Cu/Co}}$. Furthermore, Fig. 2 revealed the absence of a magnetic dead layer ($t_{\text{eff}} = 1.4\,\text{nm}$) for Cu/Pt($t_{\text{Pt}}$)/Co(1.4 nm)/Cu, which allows us to calculate the thickness of the magnetic dead layer for Cu/Co(1.4 nm)/Pt(t_{Pt})/Cu, found to be 0.25 nm ($t_{\text{eff}} = 1.15\,\text{nm}$). Finally, one obtains $K_s^{\text{Pt/Co}} = 0.5 \pm 0.05\,\text{erg/cm}^2$ and $K_s^{\text{Co/Pt}} = 0.29 \pm 0.04\,\text{erg/cm}^2$ for the two interfaces, respectively. The weak K_s for the Co/Cu interface is supported by the fact that the total interface anisotropy measured in the Ta/Co/Cu/Pt stack is only $0.2\,\text{erg} \cdot \text{cm}^{-2}$ [18]. The K_s value for the Pt/Co interface is slightly lower than the previously reported one, found to be in the range 0.6–1.4 erg/cm^2 [30], and seems to be underestimated, most likely due to the overestimated K_v value.

TABLE I. Parameters obtained from the best fits of the Ir and Pt thickness dependences of the effective PMA and the surface iDMI constants of Co thin films grown on Si substrates using Ir or Pt under or overlayer with $y = A_0 + A_1(1 - e^{-t/\lambda})$, where $t = t_{\text{Pt}}$ or t_{Ir}. ND refers to not determined due to the invariance of K_{eff} or D_s with the HM thickness.

	K_{eff} ($\times 10^6$ erg/cm^3)			D_s(pJ/m)		
System	A_0	A_1	λ (nm)	A_0	A_1	λ (nm)
Cu/Co/Pt/Cu	6.23 ± 0.1	1.81 ± 0.2	0.42 ± 0.06	0.136 ± 0.002	0.86 ± 0.01	0.36 ± 0.01
Cu/Pt/Co/Cu	6.21 ± 0.12	3 ± 0.2	0.96 ± 0.16	0.137 ± 0.011	−1.84 ± 0.08	1.43 ± 0.1
Pt/Co/Ir/Cu	12.49 ± 0.26	2.88 ± 0.4	0.34 ± 0.08	−1.2 ± 0.08	0.41 ± 0.08	0.22 ± 0.08
Pt/Cu/Ir/Co/Cu	6.21 ± 0.31	5.13 ± 0.49	0.44 ± 0.1	ND	ND	ND
Pt/Cu/Co/Ir/Cu	6.19 ± 0.17	2.84 ± 0.21	0.27 ± 0.05	0.1634 ± 0.1	0.47 ± 0.1	0.12 ± 0.1
Pt/Ir/Co/Cu	12 ± 0.42	ND	ND	−1.22 ± 0.13	1.46 ± 0.16	0.29 ± 0.08

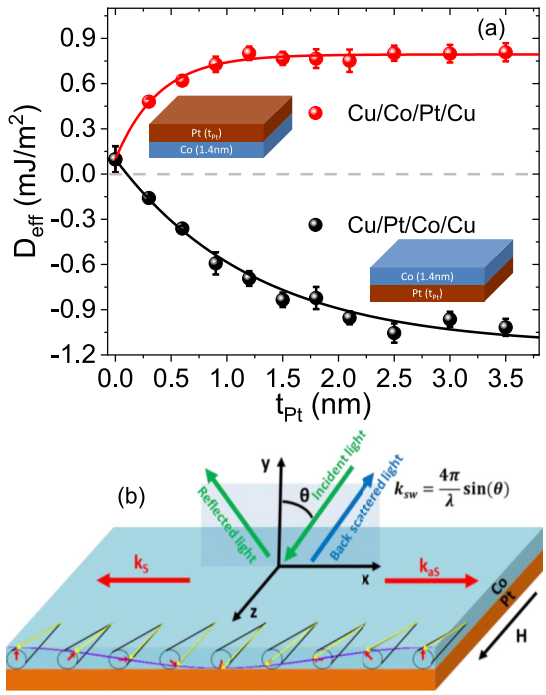

FIG. 5. Variations of (a) the effective interfacial Dzyaloshinskii-Moriya interaction (iDMI) constant (D_{eff}) vs the Pt thickness for Cu/Co(1.4 nm)/Pt(t_{Pt}) and Cu/Pt(t_{Pt})/Co(1.4 nm)/Cu systems. D_{eff} values were extracted from the fit of the spin-wave vector dependence of the frequency mismatch ΔF for Stokes (S) and anti-Stokes (aS) lines. Symbols refer to experimental data, while solid lines are fits using Eq. (5) and parameters in Table I. (b) Schematic for the chirality of spin waves inside a magnetic film in the Damon-Eshbach geometry. One first must define the oriented film normal (y) from a chosen reference layer to the film (usually the reference layer is the heavy metal whose spin-orbit interaction gives rise to iDMI). The wave vector of the spin wave is k_{sw}. A snapshot of the precessing moments for the depicted orientations of the vectors k_{sw} and static magnetization, corresponding to a counterclockwise cycloid, is also shown.

iDMI was also investigated by BLS in both systems through the measurement of the spin-wave vector (k_{sw}) dependence of the frequency mismatch ΔF which was then fitted by Eq. (4) to determine the effective constant D_{eff}, characterizing the iDMI strength:

$$\Delta F = D_{\text{eff}}\frac{2\gamma}{\pi M_s}k_{sw} = D_s\frac{2\gamma}{\pi M_s t_{\text{eff}}}k_{sw}, \tag{4}$$

where $D_{\text{eff}} = D_s/t_{\text{eff}}$ and D_s are the iDMI effective and surface constants, respectively, characterizing the iDMI strength.

Figure 5(a) shows the t_{Pt} dependence of D_{eff} for both Pt underlayer and Pt overlayer systems using $M_s = 1420\,\text{emu/cm}^3$, where a similar trend to damping and K_{eff} is observed. Here, again, D_{eff} increases in absolute values with t_{Pt} and saturates at given value which is Pt position dependent: the saturation D_{eff} value and the corresponding t_{Pt} are higher when Co is grown on top of Pt. This behavior cannot be explained by the Pt thickness dependence of M_{sn}, as mentioned above. It is most likely due to the asymmetric top and bottom interfaces of Pt with Co, presenting different intermixing degrees. One should mention that the opposite sign of D_{eff} with respect to the stack order, confirming the interfacial origin of the iDMI and its asymmetric nature, is consistent with the three-site indirect exchange mechanism [31]. To overcome the incertitude on t_{Pt} dependence of both t_{eff} and M_s and thus for more precise characterization of the iDMI strength, it is better to deal with D_s which is proportional to $t_{\text{eff}} \times M_s$, directly obtained from VSM by dividing the measured m_s by the Co film surface ($t_{\text{eff}} \times M_s = M_{sn} \times t_{\text{Co}}$, where $t_{\text{Co}} = 1.4\,\text{nm}$). Also, D_s (not shown here) behaves similarly to D_{eff}, and it is not significantly affected by Co thickness variation due to the intermixing, especially at the Co/Pt interface. The obtained D_s value at saturation for Cu/Pt/Co/Cu and Cu/Co/Pt/Cu are found to be -1.57 ± 0.07 and 1 ± 0.01 pJ/m, confirming the asymmetry of Pt/Co and Co/Pt interfaces. It seems that the higher intermixing degree at the Co/Pt interface reduces the iDMI strength and enhances the asymmetry between these interfaces. The obtained value for Cu/Pt/Co/Cu is in good agreement with the reported value for Pt/Co/AlO_x [23].

We should mention that iDMI can induce chiral spin structures, where the spatial chirality is fixed by the iDMI sign. Indeed, as shown in Fig. 5(b), when the transferred optical wave vector (along x), the applied field (along z), and the film normal from HM (Pt or Ir in this paper) to Co (along y) form a right-handed reference frame, the Stokes ($k_S = -k_{sw}$, i.e, k_S along $x < 0$) and anti-Stokes ($k_{aS} = k_{sw}$, i.e, k_{aS} along $x > 0$) spin waves correspond to a left-handed (counterclockwise) and right-handed (clockwise) cycloids, respectively. In Damon-Eshbach configuration and in the presence of iDMI, the spin-wave frequency is $F_{S,\,aS} = F \pm \Delta F = F \pm D_{\text{eff}}\frac{2\gamma}{\pi M_s}k_{sw}$, where $F_{S,aS}$ refers to $F_S (F_S = F + \Delta F)$ or F_{aS} ($F_{aS} = F - \Delta F$), and F is the spin-wave frequency in the absence of the DMI (mean frequency of F_S or F_{aS}). The spin-wave spatial chirality is favored by the iDMI if its frequency is reduced, whereas its frequency is increased for opposite chirality. As the convention adopted in this paper corresponds to $\Delta F = F_S - F_{aS}$, the iDMI constant is negative for $F_{aS} > F_S$, i.e., left-handed cycloids are favored, whereas right-handed (clockwise) helical structures are produced for positive iDMI.

We phenomenologically fitted the t_{Pt} dependences of K_{eff} and D_{eff}, shown in Figs. 4(b) and 5(a), and of D_s (not shown here) with the exponential function given by

$$y = A_0 + A_1\left[1 - \exp\left(-\frac{t_{\text{Pt}}}{\lambda}\right)\right], \tag{5}$$

where y refers to K_{eff} or D_{eff}, A_0 gives K_{eff} or D_{eff} for Cu/Co(1.4 nm)/Cu, A_1 measures the extent of PMA or iDMI strength over the t_{Pt} range, and λ is the characteristic saturation thickness appearing in the exponential growth for K_{eff} or D_{eff}, i.e., the HM (Pt in this paper) thickness, above which the iDMI or PMA magnitude for given Co thickness exceeds 63% of its saturation value. The obtained values for K_{eff} and D_s are summarized in Table I, where the saturation characteristic length scale is lower than λ_{SD}. One should mention that, by comparing Eqs. (2) and (5), one should straightforwardly see that λ should be related to $\lambda_{SD}/2$. Note that the factor 2 in the exponent term in Eq. (2) describing the spin pumping assumes that spins that reflect from the Cu/Pt or Pt/Cu interfaces must traverse a total distance that is twice the thickness of the Pt layer before returning angular momentum to the

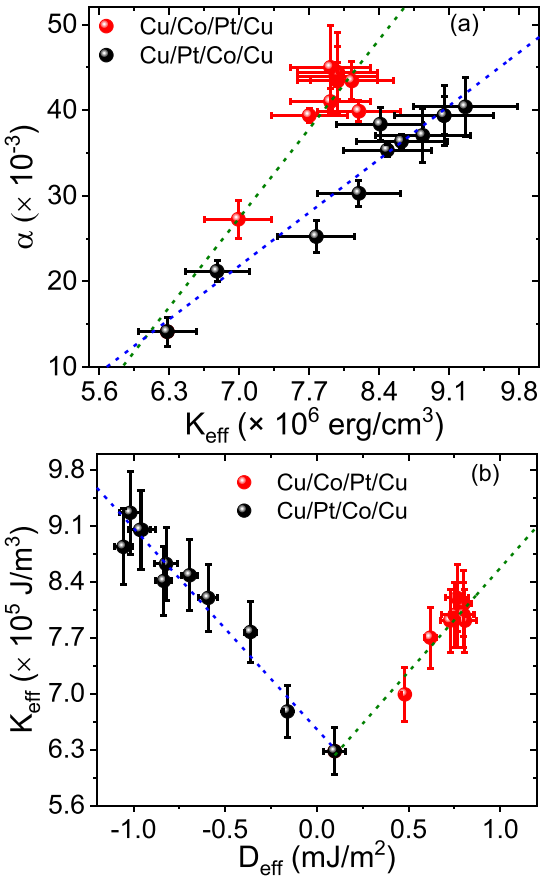

FIG. 6. (a) Variations of the damping constant (α) as a function of the effective perpendicular magnetic anisotropy (PMA) constant (K_{eff}) for Cu/Co(1.4 nm)/Pt(t_{Pt}) and Cu/Pt(t_{Pt})/Co(1.4 nm)/Cu systems. Symbols refer to experimental data, and solid lines are linear fits. (b) Variations of the perpendicular effective magnetic anisotropy constant (K_{eff}) as a function of the effective interfacial Dzyaloshinskii-Moriya interaction (iDMI) constant (D_{eff}) for Cu/Co(1.4 nm)/Pt(t_{Pt}) and Cu/Pt(t_{Pt})/Co(1.4 nm)/Cu systems with a variable Pt thickness. Symbols refer to experimental data, and the solid lines are linear fits.

Co layer. Moreover, Table I reveals that the iDMI strength is more affected by intermixing than that of K_{eff} suggesting more sensitivity of iDMI to interface quality (defect and atom arrangement at interfaces).

As mentioned above, iDMI, damping, and PMA are related to the spin-orbit interaction at the interface and are sensitive to interface properties and orbital hybridization around the Fermi level. Therefore, we investigated the eventual correlation between these quantities by plotting α vs K_{eff} and K_{eff} as a function of D_{eff}, as shown in Fig. 6 for both systems. Figure 6(a) revealed a linear correlation, which is clearer for the Cu/Pt(t_{Pt})/Co(1.4 nm)/Cu system, between K_{eff} and damping due to the second-order dependence of the two parameters with SOC, as expected theoretically. Figure 6(b) shows that K_{eff} varies linearly with D_{eff} for Cu/Pt(t_{Pt})/Co(1.4 nm)/Cu and Cu/Co(1.4 nm)/Pt(t_{Pt})/Cu systems. It is worth mentioning that a quadratic correlation between PMA and iDMI constants is theoretically predicted from perturbation theories for PMA [32] and

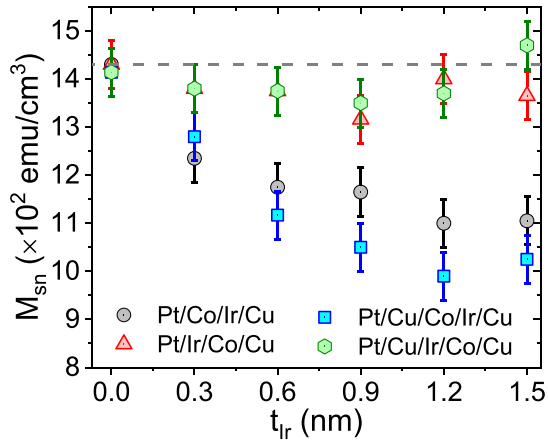

FIG. 7. Variations of the nominal magnetization at saturation (M_{sn}), calculated by dividing the measured vibrating sample magnetometry magnetic moment at saturation to the nominal volume (surface × nominal thickness) of the Co film vs the Ir thickness (t_{Ir}) of the under or overlayer in various Co- and Ir-based systems.

iDMI [33], where iDMI energy results from the first order of the SOC, whereas the PMA comes from the second order. Nevertheless, anisotropy can be influenced by other parameters such as strain or roughness. Indeed, in the Cu/Pt(t_{Pt})/Co(1.4 nm)/Cu system, residual strain that appears at the Pt/Co interface, as described above, contributes more to PMA, leading to another origin of this correlation. Indeed, Shepley *et al.* [34] reported change of 12% of the effective PMA constant for 0.1% strain in Pt/Co(1 nm)/Pt, whereas Zhang *et al.* [35] observed the enhancement of D_{eff} up to 20% for the sample with 5.5% strain for Pt/Co(3 nm)/MgO. This could explain the linear correlation between K_{eff} and D_{eff} at least for the Cu/Pt(t_{Pt})/Co(1.4 nm)/Cu system. It should be mentioned that, due to the lack of data over a larger range of iDMI in the case of Cu/Co(1.4 nm)/Pt(t_{Pt})/Cu systems, data have been fitted linearly for simplicity, although a quadratic correlation is possible. The presence of the correlation suggests the common interfaces involved in these three SOC-related effects.

C. Effect of Ir over or underlayer thickness

Four systems are considered here: Si/SiO_2/Ta(2.5)/Pt(3)/Ir(t_{Ir})/Co(1.4)/Cu(3)/Ta(2.5), referred to as Pt/Ir/Co/Cu, Si/SiO_2/Ta(2.5)/Pt(3)/Co(1.4)/Ir(t_{Ir})/Cu(3)/Ta(2.5), referred to as Pt/Co/Ir/Cu, Si/SiO_2/Ta(2.5)/Pt(3)/Cu(3)/Ir(t_{Ir})/Co(1.4)/Cu(3)/Ta(2.5), referred to as Pt/Cu/Ir/Co/Cu, and Si/SiO_2/Ta(2.5)/Pt(3)/Cu(3)/Co(1.4)/Ir(t_{Ir})/Cu(3)/Ta(2.5), referred to as Pt/Cu/Co/Ir/Cu, where Ir thickness was varied in the range 0–1.5 nm, and numbers in parentheses for both systems give the nominal thicknesses in nanometers.

Figure 7 shows the VSM nominal magnetizations at saturation (M_{sn}) for these four systems. Similarly, to the case of Pt-based samples, M_{sn} is mostly constant, over the investigated Ir thickness, when Co is grown on Ir (Pt/Ir/Co/Cu and Pt/Co/Ir/Cu systems), whereas it decreases significantly and monotonously when Ir is used as an overlayer due to

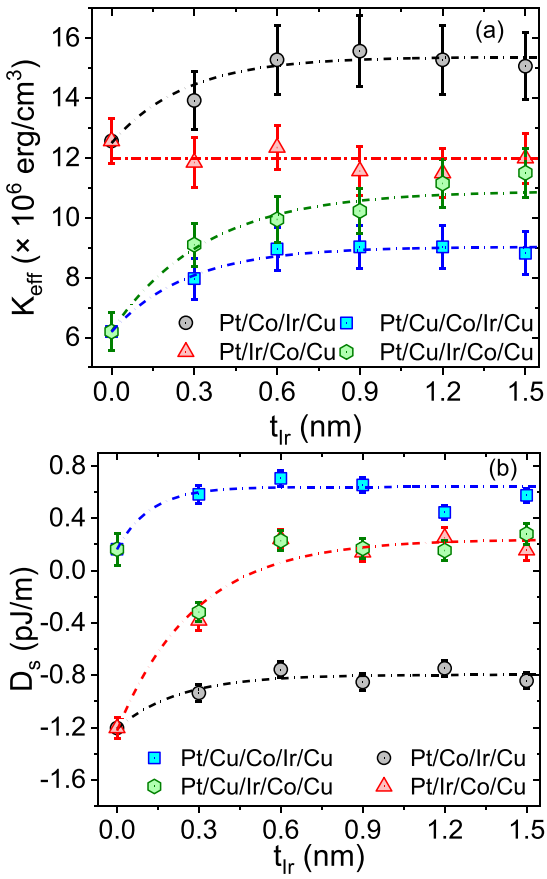

FIG. 8. Variations of (a) the effective perpendicular anisotropy constant (K_{eff}) and (b) the surface interfacial Dzyaloshinskii-Moriya interaction (iDMI) constant (D_s) vs the Ir thickness for various Co-based systems buffered or capped by Ir layers of variable thickness. Symbols refer to experimental data, while dashed lines are fits using Eq. (5) and parameters in Table I.

the increasing intermixing at the Co/Ir interface. Note the higher M_{sn} for Pt/Co/Ir/Cu than Pt/Cu/Co/Ir/Cu due to PIM at the Pt/Co interface that can be suppressed by inserting the Cu layer. Moreover, the higher extent variation of M_{sn} for Pt/Cu/Co/Ir/Cu than for Cu/Co/Pt/Cu suggests that the Ir overlayer induces more intermixing than Pt. Such intermixing difference between Ir and Pt is due to thermodynamic factors such as surface-free energies and/or cohesive energies or ballistic effects.

Figure 8(a), showing the Ir thickness dependence of K_{eff}, reveals that the Pt/Ir/Co/Cu system markedly differs from the other systems: K_{eff} is Ir thickness independent, whereas K_{eff} increases and then saturates for the three other systems. The saturation characteristic length scales, obtained from the phenomenological fit with Eq. (5) and summarized in Table I, are significantly lower than those deduced from the Pt thickness dependence, most likely due to the higher intermixing induced by Ir and the lower λ_{SD} of Ir than Pt [36]. Our data, shown in Fig. 8(a), allow us to conclude that the Ir/Co interface contribution to PMA is slightly weaker than that of Pt/Co and that the Ir underlayer induces higher PMA than the Ir overlayer, most probably due to the higher intermixing when Ir is grown on Co, as in the case of Pt samples. Furthermore, considering K_{eff} values for each system at $t_{Ir} = 0$ nm and at saturation and neglecting the contribution of the Co/Cu interface to PMA, one can obtain $K_s = 0.89$, 0.33, and 0.75 erg/cm^2 for Pt/Co, Co/Ir, and Ir/Co, respectively. Here, again, we conclude on the asymmetry of the Co/Ir and Ir/Co interfaces and the decrease of PMA of the interface where higher intermixing occurs. It is worth mentioning the higher K_s of the Pt/Co interface deduced from the Ir thickness dependence since Pt is directly grown on Ta, whereas it is grown on Cu for systems used for Pt thickness-dependence investigation. Indeed, the addition of Ta improves the roughness and facilitates the (111) texturing of the upper Pt layer and thus leads to the enhancement of the interface quality of Pt/Co, as reported by Kim *et al.* [37].

As mentioned above, using the t_{Ir} dependence of $t_{eff} \times M_s$ measured by VSM for each system, D_s was calculated from BLS measurements and is shown in Fig. 8(b) vs t_{Ir}. Interestingly, the induced iDMI by the Ir/Co interface (of negative sign like that of Pt/Co) vanishes for $t_{Ir} > 0.3$ nm for both systems involving Ir grown on Pt or on Cu, whereas iDMI resulting from the Co/Ir interface increases with t_{Ir} and then saturates for further increase of t_{Ir}. This is the opposite of what has been observed for PMA, where the Co/Ir interface is found to induce weaker PMA than Ir/Co. Note that a similar trend of the iDMI constant vs W thickness was reported by Samardak *et al.* [38]. Although the exact mechanism behind this behavior is still unknown, it is worth mentioning that iDMI is sensitive to disorder, roughness, defects, and degree of hybridization between the 3*d* orbitals of the FM metal and the 5*d* orbitals of the HM and atom arrangement at interfaces. Consequently, the different contributions of Ir/Co and Co/Ir interfaces to iDMI in our samples can be attributed to the different details of the interface morphology. The data in Fig. 8(b) were also phenomenological fitted with Eq. (5), and the characteristic parameters are summarized in Table I. The extended iDMI strength (A_1 in Table I) for Pt/Co/Ir/Cu and Pt/Cu/Co/Ir/Cu systems allows us to deduce the contribution from the top Co/Ir interface, estimated to be $D_s^{Co/Ir} = 0.4 \pm 0.1$ pJ/m. Similarly, according to Table I, the iDMI contribution of the Pt/Co interface is found to be $D_s^{Pt/Co} = -1.4 \pm 0.16$ pJ/m. The similar sign of iDMI of Co/Ir and Co/Pt interfaces is in good agreement with the previously reported trend [39]. One should mention the lower characteristic saturation length scale when Ir is the overlayer is most likely due to the stronger intermixing at this interface. Table I shows also that the saturation characteristic thickness of iDMI constant is lower than the characteristic one of K_{eff}, suggesting more localization and sensitivity of iDMI to the interface quality.

Finally, it should be mentioned that the asymmetric intermixing at interfaces of Pt and Ir with Co is not particular to our samples; it is a common feature for sputter-deposited Co/Pt and Co/Ir stacks, owing to the relatively high miscibility of the constituents. In the case of Pt/Co/Pt structures, Bandiera *et al.* [18,25] showed that, by increasing the thickness of the top Pt layer, the M_s of the stack decreases due to increased intermixing at the Co/Pt interface, as observed in our samples. Moreover, by inserting a thin Cu layer at the top Co/Pt interface, the M_s increases due to the reduction of intermixing since Co and Cu are considered immiscible. An asymmetric effect is observed when the thin Cu layer is

inserted at the bottom Pt/Co interface; the M_s decreases in this case since the Pt/Co intermixing is already negligible, and the insertion of the Cu layer only reduces the PIM. Due to the higher intermixing at the top interface, Bandiera *et al.* [25] observed an asymmetry in the interfacial anisotropies of Pt/Co and Co/Pt interfaces in Pt/Co/Pt-sputtered trilayers. Similar trends were observed by Won and Lim [40], who reported asymmetrical interface magnetic properties of Pt/Co/Pt with various Pt thicknesses due to the higher intermixing of the top Co/Pt interface, found to be greater for thicker Pt. Moreover, Lau *et al.* [41] showed a 0.2 nm increase of the magnetic dead layer for the Ir/Co/Pt structure relative to the Pt/Co/Pt one, while the magnetic dead layer increases by 0.3 nm for the Pt/Co/Ir one, which indicates asymmetric intermixing at the Ir/Co and Co/Ir interfaces, in line with our findings.

IV. CONCLUSIONS

PMA, iDMI, and Gilbert damping constants were investigated in detail vs Ir and Pt thickness in various Co-based systems with Ir or Pt under or overlayers of variable thickness. VSM revealed that Pt and Ir thickness variation results in strong intermixing at the top interface with Co, especially at Co/Ir interfaces. PMA, iDMI, and damping constants follow similar trends vs Ir and Pt thickness, where they increase and saturate. The characteristic saturation length scales are found to be dependent on heavy material and its location in the stack and seem to be linked to the spin-diffusion length of the HM. The strong intermixing at the Co/Pt interface significantly reduces the effective anisotropy constant, iDMI strength, and spin-diffusion length. Linear dependence of the damping constant α vs K_{eff} was evidenced, whereas quadratic or linear correlation between K_{eff} and D_{eff} could be found when Pt is grown on Co, in contrast to systems with a Pt buffer layer, where K_{eff} varies linearly vs D_{eff}. This different correlation between K_{eff} and D_{eff} in Pt-based systems can be attributed to the strong intermixing at the Co/Pt interface resulting in variation of the interfacial SOC. Moreover, the qualitative analysis of Ir thickness dependence of the effective PMA and iDMI constants allowed us to separate the contribution of each interface. Ir/Co is found to induce significant PMA and vanishing iDMI for Ir thickness >0.3 nm, whereas the Co/Ir interface contributes less to iDMI but induces a strong iDMI estimated to be 0.4 ± 0.1 pJ/m. This confirms the similar iDMI sign of Co/Ir and Co/Pt, leading to a subtractive behavior and thus a reduced total iDMI when they are placed on opposite sides of Co.

ACKNOWLEDGMENTS

This paper was supported by the Conseil regional d'Île-de-France (convention 1763) through the DIM NanoK (BIDUL project). M.S.G. acknowledges the financial support for this paper from MRID, CNCS/CCCDI—UEFISCDI, through Grant No. PN-III-P4-ID-PCE-2020-1853, SPINSYNE.

[1] F. Hellman *et al.*, Rev. Mod. Phys. **89**, 025006 (2017).
[2] S. Iwasaki, Proc. Jpn. Acad. Ser. B Phys. Biol. Sci. **85**, 37 (2009).
[3] L. Thomas, G. Jan, J. Zhu, H. Liu, Y-J. Lee, S. Le, R-Y. Tong, K. Pi, Y-J. Wang, D. Shen, R. He, J. Haq, J. Teng, V. Lam, K. Huang, T. Zhong, T. Torng, and P-K. Wang, J Appl. Phys. **115**, 172615 (2014).
[4] Y. C. Lee, C. T. Chao, L. C. Li, Y. W. Suen, Lance Horng, Te-Ho Wu, C. R. Chang, and J. C. Wu, J. Appl. Phys. **117**, 17A320 (2015).
[5] I. Dzyaloshinskii, J. Chem. Phys. Solids **4**, 241 (1958).
[6] T. Moriya, Phys. Rev. **120**, 91 (1960).
[7] G. Chen, T. Ma, A. T. N'Diaye, H. Kwon, C. Won, Y. Wu, and A. K. schmidt, Nature Commun. **4**, 2671 (2013).
[8] A. Fert, V. Cros, and J. Sampaio, Nat. Nanotechnol. **8**, 152 (2013).
[9] S. S. P. Parkin, M. Hayashi, and L. Thomas, Science **320**, 190 (2008).
[10] X. Zhang, M. Ezawa, and Y. Zhou, Sci. Rep. **5**, 9400 (2015).
[11] M. Benakli, A. F. Torabi, M. L. Mallary, H. Zhou, and H. N. Bertram, IEEE Trans. Magn. **37**, 1564 (2001).
[12] A. Thiaville, J. M. Garcia, and J. Miltat, J. Magn. Magn. Mater. **242–245**, 1061 (2002).
[13] I. Benguettat-El Mokhtari, D. Ourdani1, Y. Roussigné, R. B. Mos, M. Nasui, S. M. Chérif, A. Stachkevich, M. S. Gabor, and M. Belmeguenai, J. Phys. D: Appl. Phys. **53**, 505003 (2020).
[14] M. Belmeguenai, M. S. Gabor, Y. Roussigné, A. Stashkevich, S. M. Chérif, F. Zighem, and C. Tiusan, Phys. Rev. B **93**, 174407 (2016).
[15] M. S. Gabor, T. Petrisor Jr, R. B. Mos, M. Nasui, C. Tiusan, and T. Petrisor, J. Phys. D: Appl. Phys. **50**, 465004 (2017).
[16] A. L. Patterson, Phys. Rev. **56**, 978 (1939).
[17] F. Sánchez-Bajo and F. L. Cumbrera, J. Appl. Cryst. **30**, 427 (1997).
[18] S. Bandiera, R. C. Sousa, B. Rodmacq, and B. Dieny, IEEE Magn. Lett. **2**, 3000504 (2011).
[19] J. M. Shaw, H. T. Nembach, and T. J. Silva, Phys. Rev. B **85**, 054412 (2012).
[20] S. Pal, B. Rana, O. Hellwig, T. Thomson, and A. Barman, Appl. Phys. Lett. **98**, 082501 (2011).
[21] L. Zhu, D. C. Ralph, and R. A. Buhrman, Phys. Rev. Lett. **123** 057203 (2019).
[22] W. Zhang, V. Vlaminck, J. E. Pearson, R. Divan, S. D. Bader, and A. Hoffmann, Appl. Phys. Lett. **103**, 242414 (2013).
[23] M. Belmeguenai, J-P. Adam, Y. Roussigné, S. Eimer, T. Devolder, J-V. Kim, S. M. Cherif, A. Stashkevich, and A. Thiaville, Phsy. Rev. B **91**, 180405(R) (2015).
[24] K. Kyuno, F-G. Ha, R. Yamamoto, and S. Asano, J. Appl. Phys. **79**, 7084 (1996).
[25] S. Bandiera, R. C. Sousa, B. Rodmacq, and B. Dieny, Appl. Phys. Lett. **100**, 142410 (2012).
[26] V. W. Guo, B. Lu, Xi. Wu, G. Ju, B. Valcu, and D. Weller, J. Appl. Phys. **99**, 08E918 (2006).
[27] P. Bruno and J-P. Renard, Appl. Phys. A **49**, 499 (1989).
[28] M. T. Johnson, P. J. H. Bloemen, F. J. A. den Broeder, and J. J. de Vries, Rep. Prog. Phys. **59**, 1409 (1996).
[29] J. Camarero, J. J. de Miguel, R. Miranda, V. Raposo, and A. Hernando, Phys. Rev. B **64**, 125406 (2001).

[30] B. Dieny and M. Chshiev, Rev. Mod. Phys. **89**, 025008 (2017).
[31] A. Fert, Mat. Sc. Forum **59–60**, 439 (1990).
[32] P. Bruno, Phys. Rev. B **39**, 865 (1989).
[33] M. Heide, G. Bihlmayer, and S. Blügel, Physica B **404**, 2678 (2009).
[34] P. M. Shepley, A. W. Rushforth, M. Wang, G. Burnell, and T. A. Moore, Sci. Rep. **5**, 7921 (2015).
[35] W. Zhang, B. Jiang, L. Wang, Y. Fan, Y. Zhang, S. Y. Yu, G. B. Han, G. L. Liu, C. Feng, G. H. Yu, S. S. Yan, and S. Kang, Phys. Rev. Appl. **12**, 064031 (2019).
[36] T. Fache, J. C. Rojas-Sánchez, L. Badie, S. Mangin, and S. Petit-Watelot, Phys. Rev. B **102**, 064425 (2020).
[37] N-H. Kim, D-S. Han, Ji. Jung, J. Cho, J-S. Kim, H. J. M. Swagte, and C-Y. You, Appl. Phys. Lett. **107**, 142408 (2015).
[38] A. Samardak, A. Kolesnikov, M. Stebliy, L. Chebotkevich, A. Sadovnikov, S. Nikitov, A. Talapatra, J. Mohanty, and Al. Ognev, Appl. Phys. Lett. **112**, 192406 (2018).
[39] N.-H. Kim, J. Jung, J. Cho, D.-S. Han, Y. Yin, J.-S. Kim, H. J. M. Swagten, and C.-Y. You, Appl. Phys. Lett. **108**, 142406 (2016).
[40] Y. C. Won and S. H. Lim, Sci. Rep. **11**, 10779 (2021).
[41] Y-C. Lau, Z. Chi, T. Taniguchi, M. Kawaguchi, G. Shibata, N. Kawamura, M. Suzuki, S. Fukami, A. Fujimori, H. Ohno, and M. Hayashi, Phys. Rev. Materials **3**, 104419 (2019).